

# (1 + 1)-Dimensional modulation instability of spatially incoherent light

**Detlef Kip**

*Department of Physics and Solid State Institute, Technion, Haifa 32000, Israel,  
and Department of Physics, University of Osnabrück, 49069 Osnabrück, Germany*

**Marin Soljačić**

*Department of Physics, Massachusetts Institute of Technology, Cambridge, Massachusetts 02139*

**Mordechai Segev**

*Department of Physics and Solid State Institute, Technion, Haifa 32000, Israel,  
and Department of Electrical Engineering, Princeton University, Princeton, New Jersey 08544*

**Suzanne M. Sears**

*Department of Physics, Princeton University, Princeton, New Jersey 08544,  
and Department of Electrical Engineering and Computer Science, Lehigh University, Bethlehem, Pennsylvania 18015*

**Demetrios N. Christodoulides**

*Department of Electrical Engineering and Computer Science, Lehigh University, Bethlehem, Pennsylvania 18015*

Received May 31, 2001; revised manuscript received September 6, 2001

We present a comprehensive study of the one-dimensional modulation instability of partially spatially incoherent light in noninstantaneous self-focusing media. For this instability to occur, the nonlinearity has to exceed a specific threshold that depends on the coherence properties of the beam. Above this threshold a uniform-intensity partially spatially coherent wave front becomes unstable and breaks up into periodic trains of one-dimensional stripes. © 2002 Optical Society of America  
OCIS codes: 190.5530, 190.5940.

## 1. INTRODUCTION

Modulation instability (MI) is a universal process that is inherent to most nonlinear wave systems in nature.<sup>1–12</sup> Because of MI, small amplitude perturbations that originate from noise on top of a homogeneous wave front grow rapidly under the combined effects of nonlinearity and diffraction. As a result, a plane wave or a broad optical beam starts to disintegrate during propagation.<sup>1–4</sup> This disintegration in turn results in spatial filamentation of the wave and breakup into narrow beamlets. In a way entirely analogous to this process, in the temporal domain a quasi-cw pulse breaks up into a train of short pulses that are driven by the combined action of self-phase modulation and dispersion.<sup>5–12</sup> It is important to note that MI typically occurs in the same parameter region where another universal entity, a *soliton*, is observed. Solitons are localized wave packets that show no broadening during propagation in nonlinear media and, as their name suggests, behave in many cases like real particles.<sup>13</sup> For example, solitons preserve their identity and conserve their characteristics, i.e., total energy and momentum, even when they interact (collide) with one

another. The formation of spatial solitons can be intuitively understood as a result of an exact balance between the tendency to broaden because of diffraction and nonlinear self-focusing. Similarly, temporal solitons form when the natural (chromatic) dispersion is exactly compensated by nonlinear self-phase modulation effects. According to this picture, a soliton forms when the localized wave packet induces a potential well and, at the same time, becomes trapped in it, thus becoming a bound state in its own induced potential. In the spatial domain of optics a spatial soliton forms when a very narrow optical beam locally increases the refractive index, thereby inducing an optical waveguide and then becoming guided in its own induced waveguide. The relation between MI and solitons is best seen in the fact that the filaments that emerge from the MI process are actually trains of almost ideal solitons.<sup>5,14,15</sup> Therefore MI can be considered to be a precursor to soliton formation.

Over the years MI has been systematically investigated in connection with numerous nonlinear processes. However, it was always believed that MI is inherently a coherent process, and thus it can appear only in nonlinear systems with a perfect degree of spatial and temporal

coherence. On the other hand, recent theoretical<sup>16</sup> and experimental<sup>17,18</sup> work has proved that MI can also occur with partially spatially incoherent light. The implication of this result is that MI can appear in almost any weakly correlated nonlinear wave system.<sup>16</sup> The main feature of incoherent MI is the presence of a well-defined threshold: Incoherent MI appears only if the nonlinearity exceeds a specific threshold that depends on the coherence properties of the light. The appearance of a threshold for the occurrence of MI is unique to incoherent (or partially correlated) systems: MI in coherent systems has no threshold.<sup>19,20</sup> Intuitively, this threshold can be understood as the balance point between two opposing evolution processes: the nonlinear growth of periodic perturbations on top of the uniform wave front (caused by self-focusing) and the linear washout of the perturbation that results from the incoherence. Below the threshold any small periodic perturbations (in the time-averaged intensity) on top of a uniform background diminish because the diffusive washout is stronger than the nonlinear growth. Above the threshold value there is a net increase in the modulation depth (the visibility), and as a result the perturbations are amplified. On the other hand, for coherent wave fronts there is no such threshold for MI formation. The reason is simple: In linear, fully coherent systems there is no washout because the modulation depth of a periodic perturbation remains constant. Thus, in a coherent self-focusing system, such a perturbation can only grow, and, indeed, it always increases exponentially. This is why coherent MI has no threshold, and even small values of nonlinearity amplify perturbations, thereby producing MI.

The discovery of incoherent MI (the occurrence of MI in a system without perfect correlation) has implications for many other nonlinear processes beyond optics. It implies that in other nonlinear systems of weakly correlated particles one-dimensional (1D) and two-dimensional (2D) patterns can form spontaneously from noise when the nonlinearity is larger than a threshold value. The correlation distance of the multiparticle ensemble determines the threshold value. Examples of such nonlinear weakly correlated many-body systems are electrons in semiconductors in the vicinity of the quantum Hall regime, high- $T_c$  superconductors, atomic gases at temperatures slightly above the Bose–Einstein condensation temperature, or gravitational systems. Most of these systems can be described by nonlinear equations that are similar to the nonlinear wave equation in optics. Other examples include models describing nonlinear transport and weak disorder<sup>21,22</sup> that explain the large anisotropy in the conductance in 2D electron systems,<sup>23–25</sup> the Gross–Pitaevski equation for the evolution of the mean field of atomic gases,<sup>26</sup> or the governing equations of a gravitational system.<sup>27,28</sup> Charge-density waves in the form of 1D electron stripes are thought to be the reason for the anisotropic conductance,<sup>21–25</sup> and many of the properties of high- $T_c$  superconductors are attributed to stripes that form spontaneously.<sup>29,30</sup> The common features of these systems, namely, their being nonlinear, slightly disordered wave systems that give rise to patterns, suggest that the underlying physics responsible for incoherent MI is universal. Optics simply provides a

powerful tool for actually seeing the effects and isolating the different physical aspects involved.

In this paper we present a comprehensive experimental and theoretical study of the MI of partially spatially incoherent light beams in a noninstantaneous nonlinear medium. We show that self-ordered structures can form even in such systems, in spite of the imperfect coherence and the phase disorder. Incoherent MI occurs above a specific threshold that depends on the coherence properties of the beam and leads to a periodic train of 1D filaments. This study concentrates on the features of incoherent MI in a (1 + 1)D system, that is, a system with one direction of propagation and one dimension transverse to it. More specifically, we compare experimental results with the predictions of a 1D theoretical model for incoherent MI. A theoretical model explaining 2D incoherent MI and pattern formation is currently under preparation and will be presented elsewhere.<sup>31</sup>

## 2. MOTIVATION

MI is, in many aspects, closely related to the formation of spatial solitons. Therefore, before we continue to describe incoherent MI, we revisit the main ideas that lead to the formation of incoherent solitons. The existence of incoherent solitons proves that self-focusing (and, as a direct consequence, MI) is possible not only for coherent wave packets but also for wave packets for which the phase is random. Until a few years ago, solitons were considered to be solely coherent entities. However, in 1996 solitons made of partially spatially incoherent light<sup>32</sup> and in 1997 of temporally and spatially incoherent white light<sup>33</sup> were demonstrated experimentally for the first time. Since then many theoretical and experimental papers have been published on bright and dark incoherent solitons. Among such reports are investigations of the range of existence and the structure of incoherent solitons,<sup>34–43</sup> their interactions,<sup>44</sup> their stability properties,<sup>45,46</sup> and their relation to multimode composite solitons.<sup>47,48</sup> Fundamentally important for the existence of incoherent solitons is the noninstantaneous nature of the nonlinearity. Such nonlinearity responds only to the beam's time-averaged intensity structure and not to the instantaneous highly speckled and fragmented wave front. Examples of noninstantaneous media are photorefractive materials,<sup>32,49–51</sup> where charge carriers are optically excited from impurities and redistributed by different charge-transport mechanisms. After numerous cycles of excitation and retrapping (which defines the response time of the material) these charges are finally trapped in deep centers within the bandgap of the material, leading to a space-charge field that modulates the refractive index through the electro-optic effect. Another example of a noninstantaneous nonlinear medium that supports incoherent solitons are nematic liquid crystals.<sup>52</sup> Their nonlinearity relies on the slow orientational nonlinearity in which a polarized optical wave exerts a torque on the aligned molecular dipoles of a liquid crystal and orients them toward a preferential axis.<sup>53</sup>

For incoherent solitons (and incoherent MI) to occur, the response time of such a nonlinear medium must be much larger than the average time of the phase fluctua-

tions across the beam. When this condition is fulfilled, the time-averaged intensity induces, through the nonlinearity, a multimode waveguide structure whose guided modes are populated by the speckled light in a self-consistent way. With this noninstantaneous nature of the nonlinearity in mind, we were motivated to find out whether 1D and 2D patterns can form spontaneously on a partially incoherent uniform beam. As a first step, we showed theoretically<sup>16</sup> that a uniform yet partially incoherent wave front is unstable in such nonlinear media when the nonlinearity exceeds a well-defined threshold that is set by the coherence properties. According to this 1D model, above that threshold MI should occur, and patterns should form. In a recent paper<sup>17</sup> we experimentally verified these predictions. One-dimensional stripes or filaments were observed above a certain threshold of the nonlinearity, and, furthermore, at even higher values of the nonlinearity a second transition occurs, and 2D patterns of self-ordered light spots were observed. Here we continue that investigation and explore the properties of incoherent MI mainly in the region where only 1D filaments are observed, i.e., for values of the nonlinearity that are above the first threshold but still lower than the value for which 2D instability occurs. For this parameter range an experimental comparison with the corresponding 1D theoretical model is given.

### 3. THEORETICAL MODEL OF INCOHERENT MODULATION INSTABILITY

We assume that the beam propagates in the  $z$  direction, with its spatial-correlation distance being much smaller than its temporal coherence length; i.e., the beam is partially spatially incoherent and quasi-monochromatic, and the wavelength of light  $\lambda$  is much smaller than each of these coherence lengths. The nonlinear material has a noninstantaneous response; the nonlinear index change is a function of the optical intensity and is time averaged over the response time of the medium,  $\tau$ , which is much longer than the coherence time  $t_c$ . Assuming that the light is linearly polarized and that  $E(r, z, t)$  is its slowly varying amplitude, we define  $B(r_1, r_2, z) = \langle E^*(r_2, z, t)E(r_1, z, t) \rangle$ . The brackets denote the time average over time  $\tau$ . When  $r = (r_1 + r_2)/2$  and  $\rho = r_1 - r_2$  are set as the middle point and the difference coordinates, respectively,  $B(r, \rho, z)$  becomes the spatial-correlation function, with  $B(r, \rho = 0, z) = I(r, z)$  being the time-averaged intensity. Note that the definition of  $B$  implies that  $B(r, \rho, z) = B^*(r, -\rho, z)$ .

For investigation of incoherent MI, the incident light is assumed to have small time-independent perturbations  $B_1$  superimposed on an otherwise uniform intensity  $B_0$ ,  $B(r, \rho, z) = B_0(\rho) + B_1(r, \rho, z)$  with  $B_1 \ll B_0$ , where  $B_0(\rho = 0) = I_0$  is the uniform background intensity. From the paraxial wave equation,  $B$  has to fulfill<sup>16,40,41</sup>

$$\frac{\partial B}{\partial z} - \frac{i}{k} \frac{\partial^2 B}{\partial r \partial \rho} = \frac{in_0}{k} \left( \frac{\omega}{c} \right)^2 \{ \delta n(r_1, z) - \delta n(r_2, z) \} B, \quad (1)$$

where  $\omega$  is the frequency of light,  $k$  is the wave vector, and  $\delta n$  is the nonlinear refractive-index change, which is

small compared with the linear refractive index  $n_0$ . By defining  $\kappa = d[\delta n(I)]/dI$  evaluated at  $I_0$  and linearizing Eq. (1) in  $B_1$ , we find

$$\frac{\partial B_1}{\partial z} - \frac{i}{k} \frac{\partial^2 B_1}{\partial r \partial \rho} = \frac{in_0}{k} \left( \frac{\omega}{c} \right)^2 \kappa \left[ B_1 \left( r + \frac{\rho}{2}, \rho = 0, z \right) - B_1 \left( r - \frac{\rho}{2}, \rho = 0, z \right) \right] B_0(\rho). \quad (2)$$

Note that only time-independent perturbations lead to incoherent MI; time-dependent perturbations (on scales shorter than  $\tau$ ), no matter how large in amplitude they are, cannot significantly influence MI in this model, since they average out in time. The eigenmodes of Eq. (2) can be written as

$$B_1(r, \rho, z) = \exp(gz) \exp[i(\alpha r + \phi)] L(\rho) + \exp(g^*z) \exp[-i(\alpha r + \phi)] L^*(-\rho),$$

where  $\phi$  is an arbitrary real phase,  $\alpha$  is real (it is the spatial wave vector, or  $2\pi$  times the spatial frequency of the MI perturbations), and  $g$  is the growth rate of the MI at a given  $\alpha$ . These modes automatically satisfy  $B_1(r, \rho, z) = B_1^*(r, -\rho, z)$ . For each  $\alpha$  one can obtain a set of modes  $L(\rho)$  needed to describe any perturbation  $B_1$ . Defining  $M(\rho) = L(\rho)/L(\rho = 0)$ , with the boundary condition  $M(\rho = 0) = 1$ , we get

$$gM(\rho) + \frac{\alpha}{k} \frac{dM(\rho)}{d\rho} + \frac{2\omega\kappa}{c} \sin\left(\frac{\rho\alpha}{2}\right) B_0(\rho) = 0. \quad (3)$$

We are interested in the growing modes (those for which the gain  $g$  has a real component). We look for the particular and for the homogeneous solutions to Eq. (3). Since we have a physical constraint requiring that  $M(\rho)$  must be bounded for large  $|\rho|$ , the homogeneous solution has to be zero for the modes that have a real part in  $g$ . Therefore, by seeking a particular solution of Eq. (3), we find

$$\hat{M}(k_x) \left( g - i \frac{\alpha}{k} k_x \right) = \frac{i\omega\kappa}{c} \left[ \hat{B}_0 \left( k_x + \frac{\alpha}{2} \right) - \hat{B}_0 \left( k_x - \frac{\alpha}{2} \right) \right], \quad (4)$$

where

$$\hat{F}(k_x) = \frac{1}{2\pi} \int_{-\infty}^{\infty} d\rho F(\rho) \exp(ik_x \rho)$$

is the Fourier transform of  $F(\rho)$  for any  $F(\rho)$ .  $M(\rho)$  obtained from Eq. (4) is clearly bounded for large  $|\rho|$ . We stipulate  $M(\rho = 0) = 1$ , or  $\int_{-\infty}^{\infty} \hat{M}(k_x) dk_x = 1$ :

$$1 = -\frac{\omega\kappa}{c} \int_{-\infty}^{\infty} dk_x \left[ \hat{B}_0 \left( k_x + \frac{\alpha}{2} \right) - \hat{B}_0 \left( k_x - \frac{\alpha}{2} \right) \right] \frac{1}{ig + \alpha k_x / k}, \quad (5)$$

which gives us a constraint that determines the dispersion relation  $g(\alpha)$  for the modes whose  $g$  has a real part, for arbitrary  $B_0(\rho)$ . Note that  $\hat{B}_0(k_x)$  is purely real, since  $B_0(\rho) = B_0^*(-\rho)$ .

It is instructive now to illustrate the solutions of Eq. (5) for a particular example that can be solved in closed form analytically. Assuming a Lorentzian  $k$  spectrum<sup>54</sup>  $\hat{B}_0(k_x) = (I_0 k_{x0}/\pi)/(k_x^2 + k_{x0}^2)$  in Eq. (5), a contour integration yields the following result for the mode that grows, if  $g$  is bigger than zero:

$$\frac{g}{k} = -(k_{x0}/k)(|\alpha|/k) + (|\alpha|/k) \left[ \frac{\kappa I_0}{n_0} - \left( \frac{\alpha}{2k} \right)^2 \right]^{1/2}. \quad (6)$$

Having found  $g(\alpha)$ , one can then easily determine the intensity of the perturbation  $I_1(r, z) = B_1(r, \rho = 0, z)$ . We define  $k_{x0}/k = \theta_0$ , where  $\theta_0$  (in radians) is the width of the angular power spectrum of the source.

Equation (6) clearly demonstrates that the MI growth rate is substantially affected by the coherence of the source. Moreover, in the limit  $k_{x0} \rightarrow 0$ , it is correctly reduced to the well-known result of coherent MI.<sup>12</sup> Even more important, Eq. (6) indicates that, for a given degree of coherence, MI occurs only when the quantity  $\kappa I_0$  exceeds a specific threshold; incoherent MI exists *only if*  $\kappa I_0/n_0 > \theta_0^2$ , whereas for  $\kappa I_0/n_0 < \theta_0^2$ , MI is *entirely eliminated*. Thus, the more incoherent a source is, the larger is the marginal index change  $\kappa I_0$  that is expected to be induced to in turn induce MI.

On physical grounds, one expects that such a threshold would exist for any physical power spectrum (i.e., not just for a Lorentzian shape); as is shown below, this prediction is confirmed from our computer simulations. One can actually find an expression for this threshold directly from Eq. (4) for an *arbitrary* power spectrum. This expression is much more tractable analytically than Eq. (5). At the threshold,  $\alpha = 0$ ,  $g(\alpha = 0) = 0$ , but also  $d(g(\alpha = 0))/d(\alpha) = 0$ , because at threshold the point  $g(\alpha = 0) = 0$  coincides with the cutoff point, that is, the highest spatial frequency  $\alpha$  for which the growth rate  $g$  is not negative. Thus, expanding Eq. (4) in terms of small  $\alpha$  and keeping only the terms of the lowest order in  $\alpha$ , one gets the following constraint that determines the relation between the parameters exactly at the threshold:

$$1 = -\frac{\kappa k^2}{n_0} \int_{-\infty}^{\infty} \frac{dk_x}{k_x} \frac{d\hat{B}_0}{dk_x}. \quad (7)$$

For a Lorentzian power spectrum this yields  $\kappa I_0/n_0 = \theta_0^2$  as expected. For a Gaussian power spectrum  $\hat{B}_0(k_x) = [I_0/k_{x0}(\pi)^{1/2}] \exp[-(k_x/k_{x0})^2]$ , it gives  $2\kappa I_0/n_0 = \theta_0^2$ . We note that a similar method for calculating the threshold for the transverse instability of (1 + 1)D solitons in bulk media was demonstrated recently.<sup>46</sup> In Ref. 46 the solitons were fully coherent in the trapping dimension and uniform yet partially incoherent in the other transverse coordinate. When the beam is sufficiently incoherent, the transverse instability is completely eliminated.

Coming back to incoherent MI, one can find a closed-form expression for the spatial frequency  $\alpha$  that grows the fastest; let us denote this  $\alpha_{\max}$ . In addition to the

threshold relation,  $\alpha_{\max}$  is probably the only other uncomplicated experimentally measurable quantity. To derive this relation, we start from Eq. (4), take the derivative of the whole equation with respect to  $\alpha$ , and evaluate the equation at  $\alpha_{\max}$ , noting that  $dg/d\alpha = 0$ . This gives us the constraint

$$1 = -\frac{k^2 \kappa}{n_0} \int_{-\infty}^{\infty} \frac{dk_x}{k_x} \frac{d}{d\alpha} \left[ \hat{B}_0 \left( k_x + \frac{\alpha}{2} \right) - \hat{B}_0 \left( k_x - \frac{\alpha}{2} \right) \right]_{\alpha_{\max}}. \quad (8)$$

We now adapt the above general theoretical framework for our particular experimental system. When the input signal beam is uniform with intensity  $I_0$ , the underlying nonlinearity is of the form<sup>49-51</sup>

$$\delta n = \Delta n_0 \left( 1 + \frac{I_0}{I_{\text{sat}}} \right) \frac{I(r)}{I(r) + I_{\text{sat}}}, \quad (9)$$

where  $I(r)$  is the local intensity and  $I_{\text{sat}}$  is the intensity of the incident background beam. Here  $\Delta n_0 = 0.5n_e^3 r_{33}(V/L)$  is the electro-optic refractive-index change,  $n_e$  is the extraordinary refractive index,  $r_{33}$  is the electro-optic tensor element, and  $V/L$  is the externally applied electric field. Note that the actual index change is equal to  $1 - \Delta n$ ; the 1 merely rescales the bias refractive index  $n_e$ . The extra term  $1 + (I_0/I_{\text{sat}})$  comes from the fact that the total current flowing through the crystal is approximately the photocurrent generated by both beams. Therefore this form of the nonlinearity has no saturable nature. Moreover, for large input intensity  $I_0$  the extra term allows for nonlinear refractive-index changes  $\delta n$  that can be significantly larger than  $\Delta n_0$ . This possibility has to be distinguished from the case of bright screening solitons, where the soliton beam is very narrow compared with the crystal width and thus does not affect the photocurrent, and the extra term in Eq. (9) is equal to unity.<sup>49-51</sup>

Assuming a Lorentzian power spectrum, we get the following expression for  $\alpha_{\max}$ :

$$\frac{\alpha_{\max}}{k} = \left[ 2A - \frac{\theta_0^2}{2} - (2A\theta_0^2 + \theta_0^4/4)^{1/2} \right]^{1/2}, \quad (10)$$

with  $A = \kappa I_0/n_e$ . The spatial frequency  $f_{\max}$  (number of stripes per unit length in the MI pattern) is related to  $\alpha_{\max}$  by  $\alpha_{\max} = 2\pi f_{\max}$  and can be measured directly in the experiment (see Section 4).

For the form of the nonlinearity described in Eq. (9), we get  $\kappa = \Delta n_0/(I_{\text{sat}} + I_0)$ . Therefore, for large intensities  $I_0 \gg I_{\text{sat}}$ , the threshold for MI does not depend on input intensity  $I_0$ , provided that the maximum index change and spatial correlation length are held constant. The situation changes when we assume a saturable nonlinearity of the form

$$\delta n = \Delta n_0 \frac{I(r)}{I(r) + I_{\text{sat}}}. \quad (11)$$

(The photorefractive screening nonlinearity is, once again, in reality equal to  $1 - \Delta n$ , but the 1 merely rescales the bias refractive index  $n_e$ .) Now we get  $\kappa = \Delta n_0 I_{\text{sat}}/(I_{\text{sat}} + I_0)^2$ . Obviously, saturating the non-

linearity, while again keeping the maximum index change and spatial correlation distance fixed, decreases the growth rate of the MI and may lead to a complete elimination of MI. This is an important result for incoherent MI and is discussed in more detail at the end of Section 4.

#### 4. EXPERIMENTAL METHODS

In our experiments in incoherent MI, we use a photorefractive strontium barium niobate (SBN:60) crystal. The sample has been slightly doped with rhodium to enhance the photorefractive sensitivity. The dimensions of the crystal are  $a \times b \times c = 7.0 \text{ mm} \times 6.5 \text{ mm} \times 8.0 \text{ mm}$ , where light propagates along the crystalline  $a$  axis. An external electric bias field is applied along the ferroelectric  $c$  axis with silver-painted electrodes. The dominant charge-transport mechanism is electron drift in the external electric field.<sup>49–51</sup> At moderate continuous wave (cw) intensities ( $1 \text{ W/cm}^2$ ) the response time of our crystal is  $\tau \approx 0.1 \text{ s}$ . Thus, for any light beam across which the phase fluctuations are much faster than this time constant, the SBN:60 crystal responds only to the time-averaged intensity structure. In our experimental setup we split a cw argon-ion laser beam (wavelength  $\lambda = 514.5 \text{ nm}$ ) into two beams with a polarizing beam splitter. Each beam is sent through a rotating diffuser, which introduces a random phase varying much faster than the time constant  $\tau$  of the sample, thus acting as a source of partially spatially incoherent light.<sup>55</sup> Following the rotating diffusers the beams are expanded, then collimated by a set of lenses, and recombined by another polarizing beam splitter. Finally, both beams are launched into the crystal and copropagate in it. The time-averaged intensity is adjusted to be almost homogeneous over the crystal's input face, with variations being smaller than 10%. When an external dc field is applied to the crystal, the extraordinarily polarized beam experiences a significant refractive-index change. It thus serves as the signal beam, whereas the ordinarily polarized beam experiences only a tiny index change and serves as a background beam. The only role of the ordinarily polarized beam is to tune the degree of saturation of the nonlinearity.<sup>49–51</sup> A lens and a polarizer are used to image the signal beam intensity at the output face of the sample onto a CCD camera.

We control the degree of spatial coherence of the signal beam by adjusting the diameter of the laser beam incident upon the rotating diffuser: the larger the beam diameter, the higher the incoherence and the shorter the correlation distance  $l_c$ . The background beam is made highly incoherent with a correlation distance of  $\sim l_c = 8 \mu\text{m}$ , which guarantees that it never forms any patterns. We estimate the correlation distance at the input face of the crystal, when the system is linear, i.e., for zero applied field, as the average value of the full width at half-maximum (FWHM) of the speckle size on the CCD camera when the diffuser is momentarily stopped.

#### 5. EXPERIMENTAL RESULTS AND DISCUSSION

Incoherent MI is observed for a nonlinearity  $\delta n$  exceeding a certain threshold. When an external voltage is applied

to the nonlinear crystal with a magnitude large enough to allow MI, the homogeneous light distribution on the output face of the sample becomes periodically modulated and starts to form 1D filaments of incoherent light. In our experiments the preferred direction of the stripes is perpendicular to the  $c$  axis of the crystals, with some angular deviation of  $\pm 10^\circ$  from this direction. In most cases, during buildup of the filament patterns, the stripes are initially oriented perpendicular to the  $c$  axis. As the space-charge field builds up in time, the stripes rotate and move in a random way until the temporal steady state is reached. We believe that this preferred initial orientation is due to the existence of striations in our sample, which are index inhomogeneities in planes perpendicular to the  $c$  axis. The striations originate from small changes in the melt composition during growth of the crystal and may act as initial noise that is preferentially amplified by MI. These striations can be easily seen in the output intensity when the crystal is illuminated with coherent light but are almost not visible with spatially incoherent light. The typical distance between neighboring striations varies from 50 to 200  $\mu\text{m}$ . When the photorefractive space-charge field builds up and the magnitude of the nonlinearity is high enough above the MI threshold, the initial preferential periodicity of the noise makes little difference, because the nonlinear gain is high and the periodicity that grows the fastest dominates. Thus, the final periodicity of the stripes is determined primarily by the magnitude of the nonlinearity and the correlation distance and very little by the initial periodicity of the preferential noise. This fact is nicely demonstrated in our experiments by the clear observation that the final orientation of the stripes is random, with the largest observed angle of the inclination of the stripes relative to the  $c$  axis being roughly  $45^\circ$ .

In Fig. 1 we present typical examples of MI of partially spatially incoherent light. Shown is the intensity of the signal beam on the output face of the nonlinear crystal. The correlation distance of the incoherent light is  $l_c = 13 \mu\text{m}$ , and the intensity ratio is set to  $I_0/I_{\text{sat}} = 1$ . Figure 1A shows the output intensity without nonlinearity ( $V/L = 0$ ). When the nonlinearity is increased, first the threshold for 1D instability is reached in Fig. 1B. Here a mixed state can appear, in which order and disorder coexist: only parts of the crystal show filaments, while the intensity in other parts is still homogeneous.<sup>17</sup> This is an indication that the nonlinear interaction undergoes an order–disorder phase transition. Fig. 1C corresponds to a value of the nonlinearity significantly above the threshold where the filaments have been formed everywhere. When the nonlinearity is further increased, a second transition occurs: the 1D filaments become unstable (Fig. 1D) and start to break into an ordered array of 2D spots. We emphasize that in all the pictures displayed in this figure the correlation distance is much shorter than the distance between two adjacent stripes or filaments. Thus these experimental and theoretical results are a clear demonstration that patterns can also form spontaneously from noise in weakly correlated nonlinear multiparticle systems. Furthermore, as is nicely shown in Fig. 1D, even quasi-ordered patterns can form in such a random-phase, weakly correlated system. The

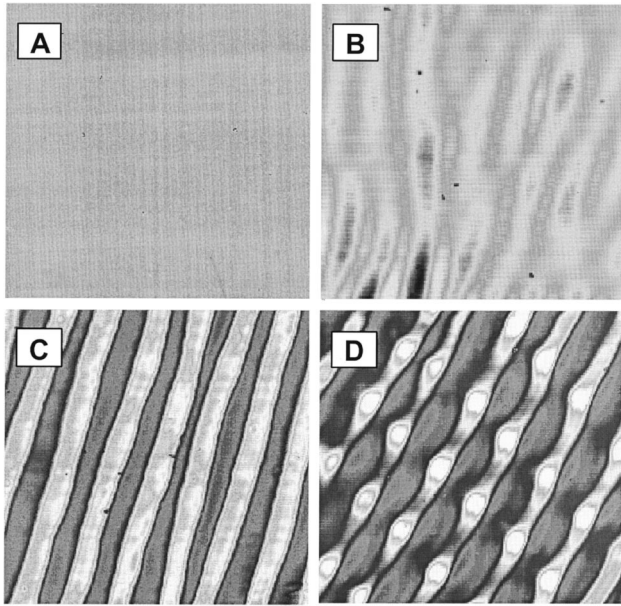


Fig. 1. Intensity structure of a partially spatially incoherent beam at the output plane of the nonlinear crystal. The sample is illuminated homogeneously with partially spatially incoherent light with a correlation distance  $l_c = 13 \mu\text{m}$ . The displayed area is  $500 \mu\text{m} \times 500 \mu\text{m}$ . The size of the nonlinear refractive-index change of the crystal is successively increased from the linear case with, A,  $\Delta n_0 = 0$  to, B,  $3.5 \times 10^{-4}$ ; C,  $5 \times 10^{-4}$ ; D,  $9 \times 10^{-4}$ . Plots B and C show the cases at threshold (with only partial features) and above threshold (features throughout) for 1D incoherent MI that leads to 1D filaments. Above this first threshold and at significantly higher values of the nonlinearity, the 1D filaments become unstable and, D, start to form a regular two-dimensional pattern.

ordered array of light spots in this figure has practically zero correlation between adjacent spots, yet the spots clearly exhibit genuine ordering.

In further experiments we concentrate on the parameter range of incoherent MI where only 1D instability is observed. For this region we can compare our results with the analytical theoretical model derived in Section 2. In the first set of measurements, we study the dependence of the MI threshold on the coherence properties of the beam. For a constant intensity ratio  $I_0/I_{\text{sat}}$ , the threshold where MI occurs depends on the correlation distance  $l_c$  of the light and on the size of  $\Delta n_0$ . To identify the MI threshold experimentally, one needs to examine the growth dynamics of perturbations of different spatial frequencies and observe whether they grow or decay. Obviously, this is very hard to measure, especially because the initial perturbations originate from striations and other noise. Instead we investigate the visibility (modulation depth) of the pattern observed at the output face of the crystal. The dominating spatial frequency of this pattern is the one that exhibits the largest gain  $g$ , as described by Eqs. (6) and (10), respectively. Random fluctuations that do not or only slightly increase have a tiny visibility and are well suppressed by the perturbations that emerge as high-visibility stripes. We conducted numerous experiments with various degrees of coherence of the input beam, and we measured the modulation depth of the output stripes as a function of the applied field, which is directly proportional to  $\Delta n_0$ . Figure 2 shows

the modulation depth  $m = (I_{\text{max}} - I_{\text{min}})/(I_{\text{max}} + I_{\text{min}})$  of the light at the output plane as a function of  $\Delta n_0$  for different correlation distances  $l_c$  and  $I_0/I_{\text{sat}} = 1$ . As is clearly shown in Fig. 2, for a fully coherent signal beam (measured without the rotating diffuser),  $m$  increases almost linearly and becomes large even for a small nonlinearity. Obviously, for the coherent case there exists no threshold for MI. When the correlation distance is reduced, however, a well-defined threshold is observed. The increase in modulation from very low visibility to high visibility is always abrupt, because for every beam with a finite  $l_c$  there is always a threshold for MI. As is shown clearly in Fig. 2, this threshold is shifted toward higher values of  $\Delta n_0$  when the correlation distance is increased.

Once the nonlinearity exceeds the threshold for incoherent MI, the transverse frequencies, which have gain, grow exponentially and form the periodic patterns shown in Fig. 1. This growth leads to a large modulation depth and high visibility of the output patterns and, at the same time, to a considerable deviation of the stripes from a pure sinusoidal shape; i.e., the propagation dynamics becomes highly nonlinear. This was already shown in Ref.

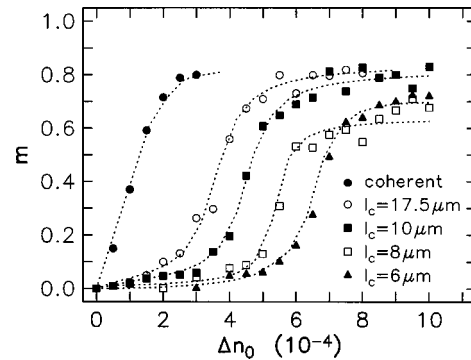


Fig. 2. Threshold dependence of incoherent MI. Shown is the modulation  $m = (I_{\text{max}} - I_{\text{min}})/(I_{\text{max}} + I_{\text{min}})$  of the light pattern as a function of the nonlinearity  $\Delta n_0$  and an intensity ratio  $I_0/I_{\text{sat}} = 1$ . The values of  $m$  are measured for correlation distances  $l_c = 6, 8, 10, 17.5 \mu\text{m}$  and for fully coherent light ( $l_c \rightarrow \infty$ ). The dotted curves are guides for the eye.

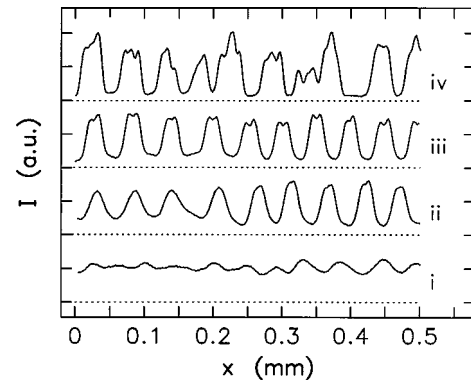


Fig. 3. Intensity cross sections of the stripes for  $l_c = 17.5 \mu\text{m}$  and nonlinear refractive-index changes  $\Delta n_0$  of, i,  $2.75 \times 10^{-4}$ ; ii,  $4 \times 10^{-4}$ ; iii,  $5 \times 10^{-4}$ ; iv,  $8 \times 10^{-4}$ . The dotted lines indicate the base line of the respective profile. The stripes emerge as sinusoidal stripes (for nonlinearity just above threshold), turn into square-wave stripes at a higher nonlinearity, and eventually break up into filaments at a large enough nonlinearity.

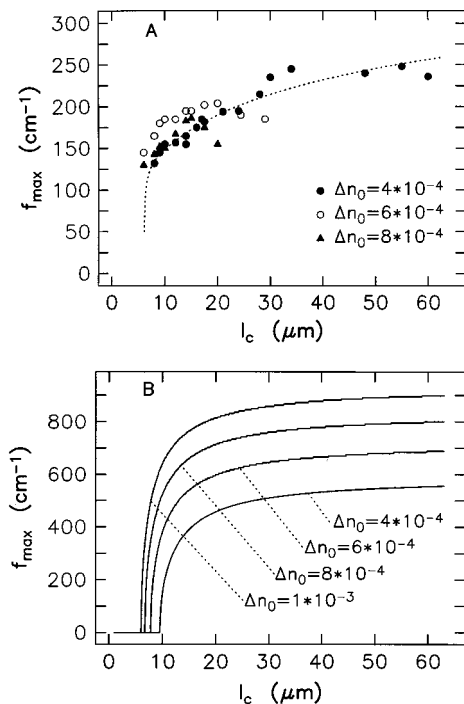


Fig. 4. Dominating spatial frequency  $f_{\max}$  (stripes per unit length) as a function of correlation distance  $l_c$ ; A, experiment; B, theory. All measured spatial frequencies are for an experimental parameter range where the 1D filaments are stable and 2D instability is not yet visible. The theoretical curves are deduced from Eq. (10) and  $\lambda = 514.5$  nm,  $n_e = 2.3$ , and  $r_{33} = 260$  pm/V. The dotted curve in A is a guide for the eye.

16; for nonlinearities high above the MI threshold, higher spatial harmonics appear in the output spectrum of the signal beam. The same behavior is observed in the experiment, as is shown in Fig. 3. At first, slightly above the threshold for 1D instability the modulation depth increases and the stripes have an almost ideal sinusoidal shape. When the nonlinearity is further increased, the shape of the stripes is no longer sinusoidal and higher harmonics are amplified, too. This is further indicated by an additional dip on top of the stripes. As already mentioned, for even a higher value of the nonlinearity the shape becomes irregular and a 2D breakup into spots is observed.<sup>17</sup>

The spatial frequency  $f_{\max}$  of the 1D filaments that emerge in the MI process depends on both the coherence properties of the beam and the magnitude of the nonlinearity. For a given intensity ratio the spatial frequency should monotonically increase with increasing correlation distance and with increasing nonlinearity. In our theoretical model this dependence is described by Eq. (10). We indeed observe this trend in our experiments. Figure 4A displays the dominant spatial frequency  $f_{\max}$  (number of stripes per unit length) of the output intensity as a function of the correlation distance  $l_c$  for a constant intensity ratio  $I_0/I_{\text{sat}} = 1$  and various values of  $\Delta n_0$ . The 1D incoherent MI theory [nonlinearity of Eq. (9), Lorentzian-shaped angular power spectrum] with the parameters  $\lambda = 514.5$  nm,  $n_e = 2.3$ , and  $r_{33} = 260$  pm/V results in the plots shown in Fig. 4B. Clearly, there is a strong qualitative agreement between theory and experiment. However, only for the lowest value of the nonlinearity

( $\Delta n_0 = 4 \times 10^{-4}$ ) are we always (i.e., for all values of  $l_c$  in our experiments) in the region where only 1D instability occurs. In this regime there is absolutely no trace of 2D instability. For the higher nonlinearities ( $6 \times 10^{-4}$  and  $8 \times 10^{-4}$ ) the 2D instability occurs for  $l_c$  values that are only slightly higher than the  $l_c$  values that are above the 1D MI threshold, so experimentally there is almost no dynamic range where 1D MI is above threshold and 2D MI is still absent. We find experimentally that when we approach the  $l_c$  value for which 2D MI starts, the values of the dominating spatial frequency slightly decreases, and obviously this behavior cannot be explained correctly by the 1D theory.

The 1D incoherent MI theory also predicts the dependence of the dominating spatial frequency  $f_{\max}$  on  $\Delta n_0$  for a given correlation distance. The corresponding measurements are shown in Fig. 5A and indeed confirm the increase of  $f_{\max}$  with increasing nonlinearity  $\Delta n_0$ . For constant, low values of the nonlinearity, higher values of  $l_c$  result in larger frequencies  $f_{\max}$ . However, experimentally we observe a turning point in the plots: The spatial frequency reaches a clear maximum and then goes down for increasing  $\Delta n_0$ . This, again, is a new feature that cannot be predicted by the 1D theory. As mentioned in the previous paragraph, in fact, for  $\Delta n_0$  values larger than those of the peaks, the 1D stripes become irregular and start to break up into 2D filaments, and this leads to a decrease in the spatial frequency of the stripes. These new unexpected effects should be addressed in the context of a 2D incoherent MI theory that also takes into account the anisotropic nature of the involved nonlinearity as well as preferential noise along the direction of the striations of the samples.

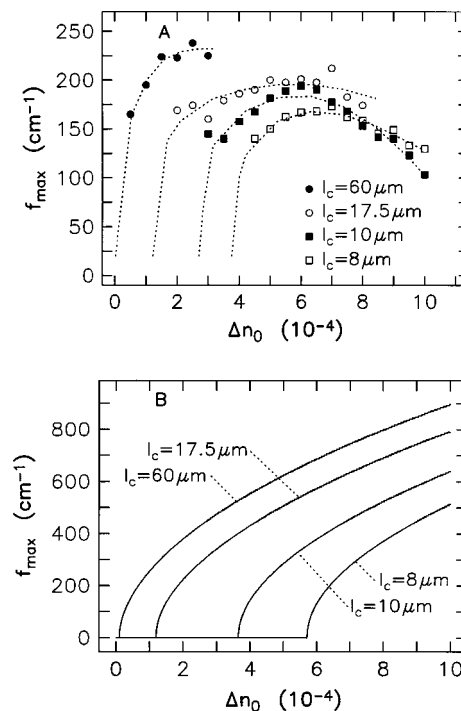


Fig. 5. Dominating spatial frequency  $f_{\max}$  as a function of nonlinear refractive-index change  $\Delta n_0$ ; A, experiment; B, theory. The dotted curves in A are guides for the eye; the theoretical curves in B are calculated with Eq. (10) and  $\lambda = 514.5$  nm,  $n_e = 2.3$ , and  $r_{33} = 260$  pm/V.

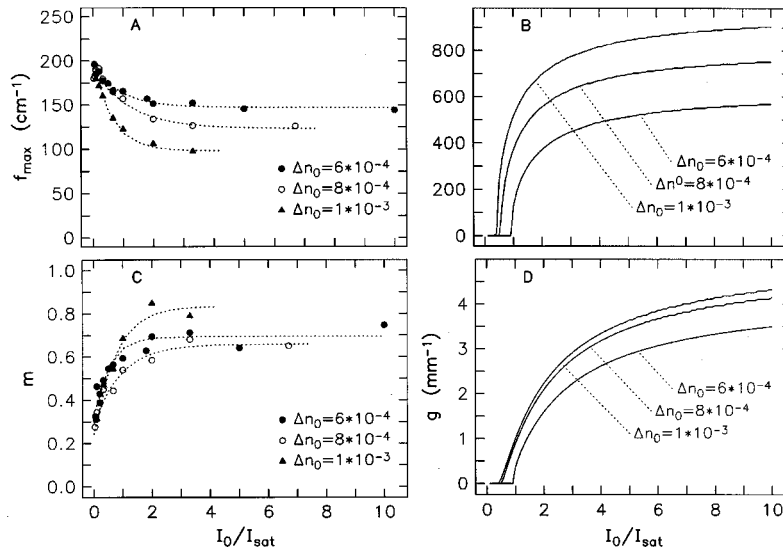


Fig. 6. Spatial frequency  $f_{\max}$ , modulation  $m$ , and gain coefficient  $g$  as a function of intensity ratio  $I_0/I_{\text{sat}}$  of signal and background beam; A, C, experiment; B, D, theory. All curves are for a spatial correlation distance  $l_c = 8 \mu\text{m}$ . The dotted curves in A and C are merely guides for the eye. The theoretical curves are deduced from Eq. (10) and  $\lambda = 514.5 \text{ nm}$ ,  $n_c = 2.3$ , and  $r_{33} = 260 \text{ pm/V}$ .

Next we investigate the dependence of frequency  $f_{\max}$  and modulation  $m$  on the ratio of signal and background beam intensity  $I_0/I_{\text{sat}}$ . All data are for a spatial correlation distance  $l_c = 8 \mu\text{m}$ . In Fig. 6A we display the dominant frequency as a function of the intensity ratio and compare these results with the theoretical curves in Fig. 6B. Here, for small intensity ratios, no clear threshold for the existence of MI is observed. However, the corresponding modulation  $m$  of the filaments starts from zero for small intensity ratios (see Fig. 6C). This is again in qualitative agreement with the growth of the exponential gain coefficient  $g$  for the frequency  $f_{\max}$  that has been calculated in Fig. 6D. More surprisingly, in the experiment the frequencies of all investigated values of the nonlinearity decrease with an increasing intensity ratio. The most likely cause of this disagreement of theory and experiment is that the theory assumes uniform initial noise, while our experimental setup in fact has preferential initial noise that is due to the striations in the material. Consequently, one expects that in the beginning of the MI evolution (which corresponds to a small nonlinearity in our experiments, keeping the length of the crystal fixed), the characteristic wavelength that will dominate the MI would be set by the characteristic size of the striations. This picture is further supported by the fact that in Fig. 6A all curves start from exactly the same  $f_{\max}$  for the low nonlinearity, as one expects; further, this  $f_{\max}$  corresponds to a length scale of  $\sim 50 \mu\text{m}$ , which is exactly the characteristic size of striations in our crystal. After some propagation distance (which is rather short in our experiments—less than 1 mm), one expects the fastest growing  $f_{\max}$  to dominate no matter what the initial noise was, and Figs. 6A and 6B seem to be consistent in this sense.

Up to this point the nonlinearity in our experiments had the form given in Eq. (9), which is not saturable. Based on the 1D incoherent MI theory,<sup>16</sup> we expect that saturation of the optical nonlinearity should arrest the MI growth rate. To investigate such saturation effects,

we have modified the nature of our photorefractive screening nonlinearity in a rather easy way. We launch a broad, nearly Gaussian beam that is still much narrower than the distance between the electrodes in our crystal, yet at the same time wide enough to serve as a quasi-uniform beam at its flat top. Since the beam is finite, it does not contribute to the total current flowing through the crystal at steady state. Hence, the nonlinearity is now that given in Eq. (11), which is the more commonly used form of the photorefractive screening nonlinearity,<sup>49–51</sup> and it is of the saturable type. When we launch such a beam in a biased crystal with  $\Delta n_0 = 6 \times 10^{-4}$ , with a correlation distance  $l_c = 13 \mu\text{m}$ , and with a ratio between the peak intensity and the saturation intensity  $I(0)/I_{\text{sat}} = 3$ , patterns form in several regions on the beam, as shown in Fig. 7A. At the almost flat center part of the beam, stripes with only a low degree of visibility appear. In this region the nonlinearity is above threshold but rather deeply saturated, causing the MI to be almost totally suppressed. However, at the tails of the beam, where the ratio  $I(r)/I_{\text{sat}}$  is lower than in the center and is near unity, stripes with high visibility appear. Obviously, in this region of the beam the nonlinearity is above threshold, so the distortions experience significant gain because of MI. Finally, at the far margins of the beam, the local nonlinearity is again below the threshold because the intensity ratio is now very low. From this particular experiment it is also evident that the 1D stripes emerge at different and rather random orientations and that this behavior is not much affected by the local noise, i.e., by the orientation of the striations that are perpendicular to the  $c$  axis.

Numerical simulations also confirm that saturation impedes the growth of MI. Using the coherent density approach,<sup>34,35</sup> we study the development of a wide beam with a peak intensity in the saturation regime, similar to the one in the experimental situation described above. The simulated beam is characterized by correlation length  $l_c = 13 \mu\text{m}$  and intensity ratio  $I(0)/I_{\text{sat}} = 3$ ; the

crystal is of length 8 mm, with a nonlinearity in the form of Eq. (11), with  $\Delta n_0 = 6 \times 10^{-4}$ . As expected, saturation inhibits MI growth in the center of the beam, while lower intensity regions on the periphery of the beam exhibit considerable striping effects (shown in Fig. 7B).

We expect that similar experiments with incoherent MI in the saturation regime of the nonlinearity, and high nonlinearities that lead to 2D lattices of filaments, will reveal a wealth of new features, because the lattice will now form features of varying order and scales in different regions of the beam. This seems to be a fascinating option, and we are currently investigating this in our laboratory.

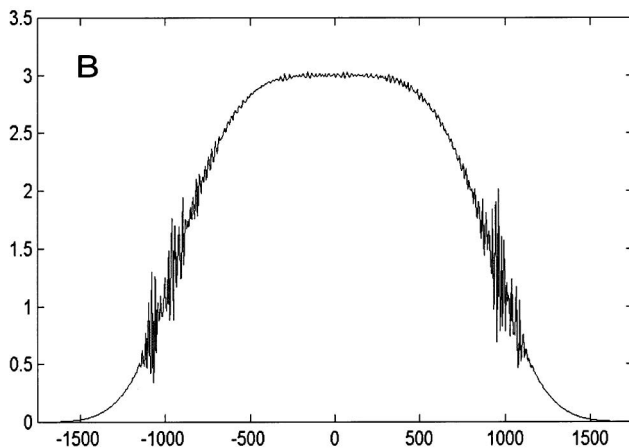
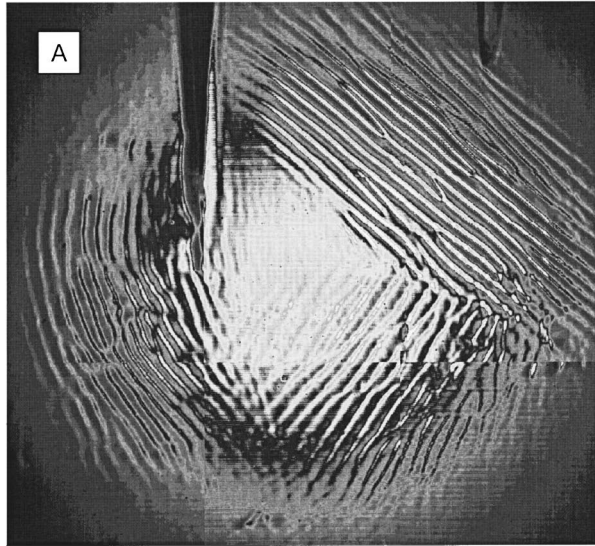


Fig. 7. Suppression of incoherent MI due to saturation of the nonlinearity. A, Intensity structure of a finite signal beam (Gaussian beam with a FWHM of 1 mm) at the output plane of the crystal. The intensity ratio (peak of beam to background intensity) is  $I_0/I_{\text{sat}} = 3$ . Without nonlinearity ( $\Delta n_0 = 0$ ), the output beam shows no features. The photograph is taken for  $\Delta n_0 = 6 \times 10^{-4}$ . The saturable nature of the nonlinearity clearly suppresses MI in the beam center, whereas strong modulation and filaments of random orientation occur in the margins of the beam. B, Intensity profile obtained with numerical simulations; this illustrates the MI inhibition caused by the saturation of the nonlinearity. Parameters match those used in the experimental configuration, with a beam intensity ratio of  $I_0/I_{\text{sat}} = 3$ , a crystal nonlinearity of the saturable form, and  $\Delta n_0 = 6 \times 10^{-4}$ . Ripples due to MI appear at the edges of the beam where the intensity tapers off.

## 6. CONCLUSION

In conclusion, we have presented detailed results of the experimental observation of the modulation instability (MI) of spatially incoherent light beams in a nonlinear optical system and compared these results with a theoretical model. We have proved that modulation instability occurs when the nonlinearity exceeds a sharp threshold. This threshold depends on the degree of coherence, i.e., on the correlation distance defined as the maximum distance between two points on the beam that are still phase correlated. We have shown that during the MI process a homogeneous input wave front breaks into one-dimensional (1D) stripes. For a higher nonlinearity, we observe a second threshold at which the stripes become unstable and spontaneously form a spatially ordered pattern of two-dimensional (2D) filaments or spots. We have qualitatively and quantitatively compared the features of incoherent MI found experimentally with those predicted theoretically. The comparison reveals a nice agreement for most features in the regime where only 1D patterns emerge. Yet neither of the experimental findings that relate to the 2D MI patterns can be explained in the framework of our current 1D theory. At this point, the necessity of a 2D MI theory, one that will also include the effects of anisotropic noise and an anisotropic correlation function (with respect to the two transverse dimensions), is clear. We have recently developed such a theory.<sup>31</sup>

In closing, we draw attention once again to the wealth of pattern formation phenomena that appear in disordered (or weakly correlated) nonlinear wave systems in numerous fields other than optics. We believe that the experimental and theoretical results will help the understanding of the general and universal properties and underlying effects in other physical systems. These include, for example, nonlinear systems of weakly correlated waves and particles, Bose–Einstein condensates, high- $T_c$  superconductors, fractional quantum Hall effects, and gravitational systems.

## ACKNOWLEDGMENT

This work was supported by the state of Lower Saxony, Germany, the Israeli Science Foundation, the National Science Foundation, the U.S. Army Research Office, and the U.S. Air Force Office of Scientific Research. It is also part of the Multidisciplinary University Research Initiative project on optical spatial solitons.

## REFERENCES AND NOTES

1. V. I. Bespalov and V. I. Talanov, "Filamentary structure of light beams in nonlinear liquids," *JETP Lett.* **3**, 307–310 (1966).
2. P. V. Mamyshev, C. Bosshard, and G. I. Stegeman, "Generation of a periodic array of dark spatial solitons in the regime of effective amplification," *J. Opt. Soc. Am. B* **11**, 1254–1260 (1994).
3. M. D. Iturbe-Castillo, M. Torres-Cisneros, J. J. Sanchez-Mondragon, S. Chavez-Cerda, S. I. Stepanov, V. A. Vysloukh, and G. E. Torres-Cisneros, "Experimental evidence of modulation instability in a photorefractive  $\text{Bi}_{12}\text{TiO}_{20}$  crystal," *Opt. Lett.* **20**, 1853–1855 (1995).
4. M. I. Carvalho, S. R. Singh, and D. N. Christodoulides, "Modulational instability of quasi-plane-wave optical

- beams biased in photorefractive crystals,” *Opt. Commun.* **126**, 167–174 (1996).
5. E. M. Dianov, P. V. Mamyshev, A. M. Prokhorov, and S. V. Chernikov, “Generation of a train of fundamental solitons at a high repetition rate in optical fibers,” *Opt. Lett.* **14**, 1008–1010 (1989).
  6. V. I. Karpman, “Self-modulation of nonlinear plane waves in dispersive media,” *JETP Lett.* **6**, 277–280 (1967).
  7. V. I. Karpman and E. M. Kreushkal, “Modulated waves in non-linear dispersive media,” *Sov. Phys. JETP* **28**, 277–281 (1969).
  8. A. Hasegawa and W. F. Brinkman, “Tunable coherent IR and FIR sources utilizing modulation instability,” *IEEE J. Quantum Electron.* **QE-16**, 694–697 (1980).
  9. K. Tai, A. Hasegawa, and A. Tomita, “Observation of modulational instability in optical fibers,” *Phys. Rev. Lett.* **56**, 135–138 (1986).
  10. G. P. Agrawal, “Modulation instability induced by cross-phase modulation,” *Phys. Rev. Lett.* **59**, 880–883 (1987).
  11. S. Wabnitz, “Modulational polarization instability of light in a nonlinear birefringent dispersive medium,” *Phys. Rev. A* **38**, 2018–2021 (1988).
  12. G. P. Agrawal, *Nonlinear Fiber Optics* (Academic, New York, 1995).
  13. For a recent review on optical spatial solitons, see G. I. Stegeman and M. Segev, “Optical spatial solitons and their interactions: universality and diversity,” *Science* **286**, 1518–1523 (1999).
  14. A. Hasegawa, “Generation of a train of soliton pulses by induced modulational instability in optical fibers,” *Opt. Lett.* **9**, 288–290 (1984).
  15. M. Artiglia, E. Ciaramella, and P. Gallina, “Demonstration of cw soliton trains at 10, 40 and 160 GHz by means of induced modulation instability,” in *System Technologies*, C. Menyuk and A. Willner, eds., Vol. 12 of OSA Trends in Optics and Photonics Series (Optical Society of America, Washington, D.C., 1997), pp. 305–308.
  16. M. Soljacić, M. Segev, T. Coskun, D. N. Christodoulides, and A. Vishwanath, “Modulation instability of incoherent beams in noninstantaneous nonlinear media,” *Phys. Rev. Lett.* **84**, 467–470 (2000).
  17. D. Kip, M. Soljacić, M. Segev, E. Eugenieva, and D. N. Christodoulides, “Modulation instability and pattern formation in spatially incoherent light beams,” *Science* **290**, 495–498 (2000).
  18. J. Klinger, H. Martin, and Z. Chen, “Experiments on induced modulational instability of an incoherent optical beam,” *Opt. Lett.* **26**, 271–273 (2000).
  19. We note the distinction between the MI threshold and the existence of a threshold for soliton formation, the former being unique to partially incoherent systems, whereas the latter can be found in many coherent systems. For example, there is a clear threshold for envelope soliton formation in weakly dissipative systems; see A. N. Slavin, “Thresholds of envelope soliton formation in a weakly dissipative medium,” *Phys. Rev. Lett.* **77**, 4644–4647 (1996).
  20. We also note that, in principle, effects that are closely related to the MI of partially incoherent wave fronts could also be observed with diffusive nonlinearities, that is, nonlinearities for which the nonlinear index change is a function of the optical intensity averaged over the characteristic diffusion length. Such diffusive effects exist in several material systems, e.g., in semiconductor lasers with free-carrier nonlinearities, where diffusion of charge carriers washes out all structures more delicate than the diffusion length. However, to our knowledge, MI in such systems has not been studied.
  21. A. A. Koulakov, M. M. Fogler, and B. I. Shklovskii, “Charge density wave in two-dimensional electron liquid in weak magnetic field,” *Phys. Rev. Lett.* **76**, 499–502 (1996).
  22. A. H. MacDonald and M. P. A. Fisher, “Quantum theory of quantum Hall smectics,” *Phys. Rev. B* **61**, 5724–5733 (2000).
  23. M. P. Lilly, K. B. Cooper, J. P. Eisenstein, L. N. Pfeiffer, and K. W. West, “Evidence for an anisotropic state of two-dimensional electrons in high Landau levels,” *Phys. Rev. Lett.* **82**, 394–397 (1999).
  24. M. P. Lilly, K. B. Cooper, J. P. Eisenstein, L. N. Pfeiffer, and K. W. West, “Anisotropic states of two-dimensional electron systems in high Landau levels: effect of an in-plane magnetic field,” *Phys. Rev. Lett.* **83**, 824–827 (1999).
  25. W. Pan, R. R. Du, H. L. Stormer, D. C. Tsui, L. N. Pfeiffer, K. W. Baldwin, and K. W. West, “Strongly anisotropic electronic transport at Landau level filling factor  $\nu = 9/2$  and  $\nu = 5/2$  under a tilted magnetic field,” *Phys. Rev. Lett.* **83**, 820–823 (1999).
  26. Th. Busch and J. R. Anglin, “Motion of dark solitons in trapped Bose–Einstein condensates,” *Phys. Rev. Lett.* **84**, 2298–2301 (2000).
  27. F. G. Bridges, A. Hatzes, and D. N. C. Lin, “Structure, stability and evolution of Saturn’s rings,” *Nature* **309**, 333–335 (1984).
  28. K. Bekki, “Group-cluster merging and the formation of starburst galaxies,” *Astrophys. J.* **510**, 15–19 (1999).
  29. V. J. Emery, S. A. Kivelson, and J. M. Tranquada, “Stripe phases in high-temperature superconductors,” *Proc. Natl. Acad. Sci. U.S.A.* **96**, 8814–8817 (1999).
  30. S. R. White and D. J. Scalapino, “Competition between stripes and pairing in a  $t$ - $t'$ - $J$  model,” *Phys. Rev. B* **60**, R753–R756 (1999).
  31. S. M. Sears, M. Soljacić, D. N. Christodoulides, and M. Segev, “Pattern formation via symmetry breaking in nonlinear weakly correlated systems,” to be published in *Phys. Rev. E*.
  32. M. Mitchell, Z. Chen, M. Shih, and M. Segev, “Self-trapping of partially spatially incoherent light,” *Phys. Rev. Lett.* **77**, 490–493 (1996).
  33. M. Mitchell and M. Segev, “Self-trapping of incoherent white light,” *Nature* **387**, 880–883 (1997).
  34. D. N. Christodoulides, T. H. Coskun, M. Mitchell, and M. Segev, “Theory of incoherent self-focusing in biased photorefractive media,” *Phys. Rev. Lett.* **78**, 646–649 (1997).
  35. D. N. Christodoulides, T. H. Coskun, M. Mitchell, and M. Segev, “Multimode incoherent spatial solitons in logarithmically saturable nonlinear media,” *Phys. Rev. Lett.* **80**, 2310–2313 (1998).
  36. M. Mitchell, M. Segev, T. H. Coskun, and D. N. Christodoulides, “Theory of self-trapped spatially incoherent light beams,” *Phys. Rev. Lett.* **79**, 4990–4993 (1997).
  37. A. W. Snyder and D. J. Mitchell, “Big incoherent solitons,” *Phys. Rev. Lett.* **80**, 1422–1424 (1998). This ray optics model of incoherent solitons is similar to the model of random-phase solitons in plasma, suggested in Refs. 38 and 39.
  38. A. Hasegawa, “Dynamics of an ensemble of plane waves in nonlinear dispersive media,” *Phys. Fluids* **18**, 77–78 (1975).
  39. A. Hasegawa, “Envelope soliton of random phase waves,” *Phys. Fluids* **20**, 2155–2156 (1977). This model assumes zero degree of coherence, that is, every single point on the beam acts as an independent point source. This view is problematic for several reasons. First, zero-correlated beams can be described neither by a paraxial equation nor by a Helmholtz equation: They require full vectorial formulation through Maxwell equations. Second, this model implies that the shape of incoherent solitons is completely arbitrary and their correlation statistical properties are delocalized, which is just an artifact of using a transport equation—see Refs. 33–35. But worse than all other artifacts of the total incoherence assumption is that such transport (or ray optics) models are modulationally stable, i.e., there is no MI in these models. The reason is obvious: The MI threshold is a function that is monotonically increasing with decreasing correlation distance. For fully spatially incoherent beams the transverse correlation distance is zero, which implies that the threshold for MI is infinity. This is obviously unphysical and is a direct artifact of the full incoherence assumption.
  40. G. A. Pasmanik, “Self-interaction of incoherent light beams,” *Sov. Phys. JETP* **39**, 234–238 (1974).
  41. V. V. Shkunov and D. Z. Anderson, “Radiation transfer

- model of self-trapping spatially incoherent radiation by nonlinear media," *Phys. Rev. Lett.* **81**, 2683–2686 (1998).
42. Z. Chen, M. Mitchell, M. Segev, T. H. Coskun, and D. N. Christodoulides, "Self-trapping of dark incoherent light beams," *Science* **280**, 889–892 (1998).
  43. D. N. Christodoulides, T. H. Coskun, M. Mitchell, Z. Chen, and M. Segev, "Theory of incoherent dark solitons," *Phys. Rev. Lett.* **80**, 5113–5116 (1998).
  44. N. Akhmediev, W. Krolikowski, and A. W. Snyder, "Partially coherent solitons of variable shape," *Phys. Rev. Lett.* **81**, 4632–4635 (1998).
  45. O. Bang, D. Edmundson, and W. Krolikowski, "Collapse of incoherent light beams in inertial bulk Kerr media," *Phys. Rev. Lett.* **83**, 5479–5483 (1999).
  46. C. Anastassiou, M. Soljačić, M. Segev, D. Kip, E. Eugenieva, D. N. Christodoulides, and Z. Musslimani, "Eliminating the transverse instabilities of Kerr solitons," *Phys. Rev. Lett.* **85**, 4888–4891 (2000).
  47. M. Mitchell, M. Segev, and D. N. Christodoulides, "Observation of multihump multimode solitons," *Phys. Rev. Lett.* **80**, 4657–4660 (1998).
  48. T. Coskun, D. N. Christodoulides, Y. Kim, Z. Chen, M. Soljačić, and M. Segev, "Bright spatial solitons on a partially incoherent background," *Phys. Rev. Lett.* **84**, 2374–2377 (2000).
  49. M. Segev, G. C. Valley, B. Crosignani, P. DiPorto, and A. Yariv, "Steady state spatial screening-solitons in photorefractive media with external applied field," *Phys. Rev. Lett.* **73**, 3211–3214 (1994).
  50. D. N. Christodoulides and M. I. Carvalho, "Bright, dark, and gray spatial soliton states in photorefractive media," *J. Opt. Soc. Am. B* **12**, 1628–1633 (1995).
  51. M. Segev, M. Shih, and G. C. Valley, "Photorefractive screening solitons of high and low intensity," *J. Opt. Soc. Am. B* **13**, 706–718 (1996).
  52. M. Peccianti and G. Assanto, "Incoherent spatial solitary waves in nematic liquid crystal," *Opt. Lett.* **26**, 1791–1793 (2001).
  53. N. V. Tabiryan, A. V. Sukhov, and B. Ya. Zel'dovich, "The orientational optical nonlinearity of liquid crystals," *Mol. Cryst. Liq. Cryst.* **136**, 1–140 (1986).
  54. A Lorentzian power spectrum shape is not physical in 2D, since it would imply a logarithmically divergent intensity. Furthermore, one has reasons to doubt that it is a physically valid solution for all  $k_x$  even in the 1D case. Nevertheless, it is a good approximation to the true shape (apart for the tails in large  $k_x$ ). Since this model can be solved in a closed form analytically, we find it to be useful for studying and understanding MI. One should compare this situation with the approximation of parabolic waveguides in optical fibers, which serve as a good approximation of true graded-index waveguides, although of course true parabolic waveguides do not exist in reality.
  55. The rotating diffuser also broadens the linewidth of the laser light, because the rotation causes a Doppler shift. In our experiments, however, the speckles introduce a new phase every microsecond, and therefore the Doppler shift is of the order of megahertz, which is negligible compared with the  $\sim 1$  GHz laser linewidth that we use.